Article

Photographic Analysis and Optical Diagnosis of Kilowatt Microwave Plasma Torch with Air Carrier Gas

YU Dengjie[1,2#], YU Bingwen[1,2#], ZHANG Xuchen[1], HUANG Shiluo[1], YING Yangwei[1], YAN Yuwei[1], JIN Yining[3] and JIN Wei[1,2✉]

Received April 25, 2023
Accepted June 25, 2023

The spatiotemporal motion characteristics of the kilowatt argon microwave plasma torch with the air carrier gas (kW-AC-ArMPT) and the behavior of the plasma filaments are investigated with a digital single-lens reflex (SLR) camera and a high-speed camera. Along with the introduction of the air, both the volume of the central channel and the rotational frequency of the plasma filament are increased. Besides, the excitation temperature (T_{exc}), rotational temperature (T_{rot}), and density of electron number (n_e) of the kW-AC-ArMPT are measured with optical diagnosis. It is clearly shown that the introduction of air contributed to the rise of T_{rot} and n_e of the plasma, which is beneficial to improving the analytical performance of the plasma. Then the detection limits of some heavy metal elements are measured by kW-AC-ArMPT, which are in the ppb range. The experimental results show that the kW-ArMPT has a high tolerance to air injection at least 1.0 L/min, which allows the direct extraction of air from the environment for analysis and therefore has the potential for online and *in-situ* detection of ambient air quality and industrial exhaust gases.

Keywords Air carrier gas; Microwave plasma torch; Photographic analysis; Optical diagnosis

1 Introduction

Argon microwave plasma torch (ArMPT) has exhibited many advantages, including stability, strong excitation capability, resistance to the injection of molecular gases and organic substances, and lower cost[1−3]. It has been successfully applied to several fields like element detection[4−9] and origin traceability[10,11].

Duan *et al*.[12] reported a low-power ArMPT with a mixed air-argon injection that can withstand an air content of up to 20% and an airflow rate of 0.2 L/min. However, the introduction of more air will lead to plasma instability or even sudden extinction. Therefore, the application in online detection is limited.

It is necessary to further improve the power and power coupling efficiency of MPT, for which Yu *et al*.[2,3] developed a dual-resonant kilowatt MPT, and Zhu *et al*.[13] further realized self-ignition by studying the resonance characteristics and electric field distribution at the open end of the torch on this basis. The improved MPT greatly increases the tolerance for air aerosols, which can work with a higher air carrier gas flow rate. This phenomenon may be explained by the fact that the plasma root and the sample inlet are spatially separated so that there is no significant interference between them, thus preserving the stability of the plasma, and that the unique central channel formed by the rotation of the discharge filament facilitates the introduction of the sample, which was found by Yu *et al*.[3] using a high-speed camera to study the spatio-temporal motion characteristics of the ArMPT.

The ability to withstand more air carrier gas expands the application range of the plasma. Ambient gases or plant exhaust gases can be collected directly with a pump and introduced into the MPT for the real-time monitoring of airborne particulate matter and heavy metal contaminants at production sites for online, *in-situ* detection without the need for complex sample pre-treatment processes.

In this paper, we studied images, basic plasma parameters and detection limits of some heavy metal elements of kilowatt ArMPT with the air carrier gas (kW-AC-ArMPT). All this above-mentioned work lays a foundation for understanding the behavior of the kW-AC-ArMPT and improving its performance, thus broadening the application fields.

2 Experimental

The experimental setup is shown schematically in Fig.1. The MPT was assembled in our laboratory, and the microwave energy was provided by a lab-made, adjustable and high-powered microwave generator (2450 MHz). Spectral data were acquired with a single-channel scanning spectrometer (NCS Testing Technology Co., Ltd., China). The carrier gas was a mixture of air and argon formed by a tee connector; the flow rate of the mixture gas was regulated separately by rotameters to adjust the air content. Argon and oxygen were used as the

✉ JIN Wei
jinweimy@zju.edu.cn
# These authors contributed equally to this work.
1. Research Center for Analytical Instrumentation, Institute of Cyber-Systems and Control, College of Control Science and Engineering, Zhejiang University, Hangzhou 310058, P. R. China;
2. Research Center for Analytical Instruments and Intelligent Systems, Huzhou Institute of Zhejiang University, Huzhou 313002, P. R. China;
3. Faculty of Engineering, University of Alberta, 116 St. and 85 Ave., Edmonton, Alberta, Canada

https://doi.org/10.1007/s40242-023-3110-5

supporting and shielding gases, respectively. All the working gases (purity of 99.999%) were provided by Hangzhou Jingong Special Gas Co., Ltd. (China). The liquid samples were pumped into the pneumatic nebulizer by a peristaltic pump to yield an aerosol sample in the cyclone spray chamber and then carried into the plasma by the mixed carrier gas. The other experimental parameters are set in Table 1 unless otherwise stated.

Two cameras were used to investigate the images of kW-AC-ArMPT at different time scales and compared with ArMPT. A single-lens reflex (SLR) camera (D5300, Nikon Corporation, Japan) was used to capture the overall images of the plasma, and a high-speed camera (NX4S3-3G, IDT, USA) was used to investigate the characteristics of the plasma discharge filaments. The exposure time of the former was set to 10 ms (defined as macroscopic time scale); meanwhile, according to the sampling theory, the frame frequency of the latter was set to 2000 Hz (0.5 ms per frame, defined as microscopic time scale), which was twice higher than the typical rotation frequency of the plasma filament[14]. The single sampling length of the high-speed camera was 200 frames (corresponding to a time of 100 ms), and the rotation frequency was calculated by counting how many times the filament rotated during the one sampling period.

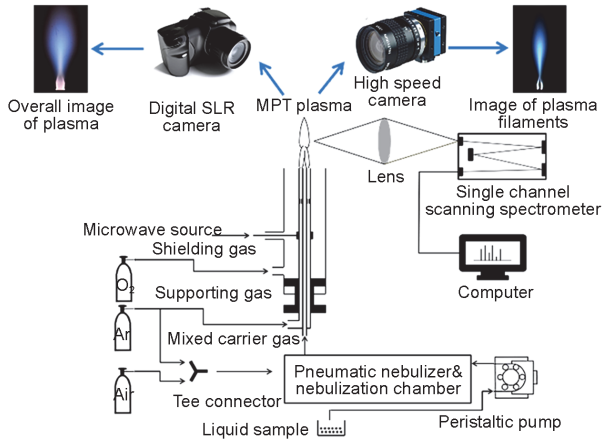

Fig.1 Schematic diagram of kilowatt MPT-atomic emission spectrometry (AES) setup

Table 1 Experimental parameters

Microwave power/W	300—1000
Air content (%)	0—100
Observation height	8 mm above the opening end of the torch
Mixed carrier gas flow rate/(L·min^{-1})	0.5
Supporting gas flow rate/(L·min^{-1})	1.0
Shielding gas flow rate/(L·min^{-1})	1.5

3 Results and Discussion

3.1 Photographic Analysis

The typical images of the plasma with air carrier gas are shown in Figs.2 and 3. Among them, Fig.2 tests the MPT's ability to endure the highest air carrier gas flow rate. The kW-ArMPT can sustain at least 1.0 L/min of pure air injection with excellent stability. When the air carrier gas flow rate is further increased, the plasma shape changes and no longer has an inverted conical structure, which causes the sample to pass directly through the plasma and not have sufficient contact with the plasma, detrimental to the analytical performance.

Compared to the argon carrier gas ArMPT, the morphology of the air carrier gas ArMPT changes from an

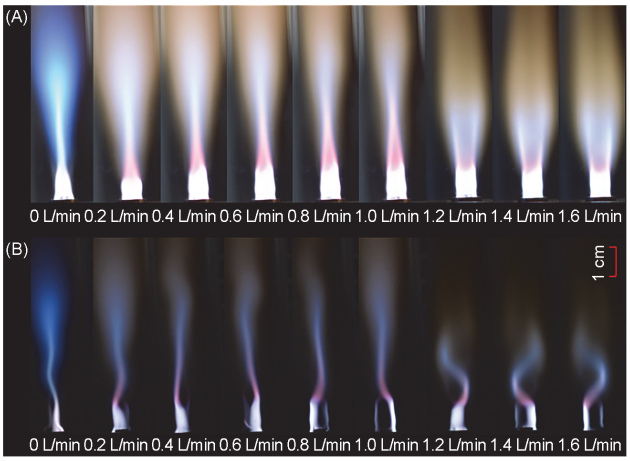

Fig.2 Variation of plasma images with air carrier gas flow rate at macroscopic (A) and microscopic (B) time scales

The microwave power is 600 W and the air content is 100%.

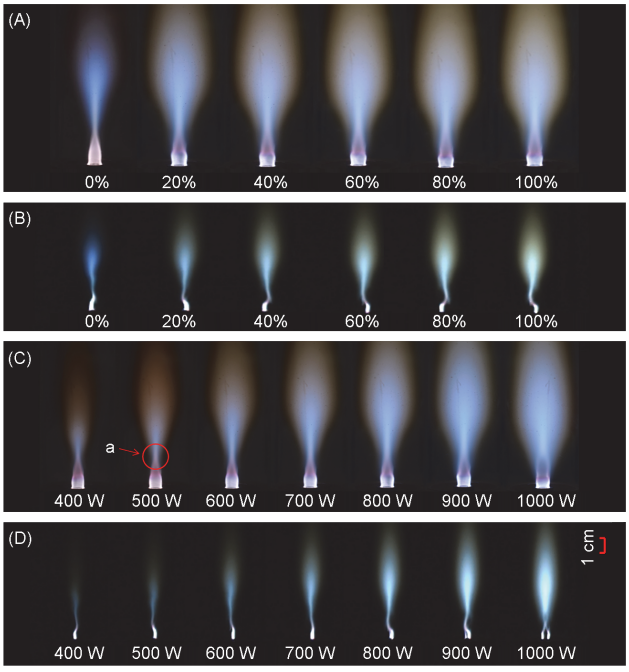

Fig.3 Variation of plasma images with air content (A, B) and with microwave power (C, D) at macroscopic (A, C) and microscopic (B, D) time scales

(A, B) The microwave power is 800 W and the carrier gas flow rate is 0.5 L/min; (C, D) the air content is 20% and the carrier gas flow rate is 0.5 L/min.

https://doi.org/10.1007/s40242-023-3110-5

inverted cone to an inverted bell shape, and also has a crossover point, as shown by the red circle 'a' in Fig.3(C).

The color near the crossover point of the plasma gradually changes from white to purple or magenta when the carrier gas gradually changes to air [Fig.3(A)]. Fig.4 compares the argon carrier gas plasma and air carrier gas plasma under the same conditions. Among them, when the carrier gas is air, the NO band with a stronger spectral intensity appears at 200—300 nm. When the carrier gas is argon, there are obvious argon lines in the spectra in 415—428 nm and 706—773 nm.

Additionally, the central channel's volume of the plasma considerably grows and remains stable, which is more conducive to the introduction of sample aerosol. On the microscopic scale, plasma is formed by single or multiple discharge filaments rotating rapidly around an axis.

To investigate the effect of microwave power on plasma, the ArMPT with 20% air content carrier gas injection is photographed in the microwave power range of 400—1000 W. As the microwave power increases [Fig.3(C)], the position of the plasma crossover point gradually shifts upward. Since the region around the plasma crossover is the core region of the sample analysis, in the practical application, the best observation region should be adjusted upward accordingly. The effect of microwave power on plasma discharge filaments is more pronounced at microscopic time scales [Fig.3(D)]. Under lower power conditions, the plasma has a single discharge filament structure rotating around the axis, and as the power increases, the width of the plasma discharge filament gradually becomes wider, and then, the plasma discharge filament gradually splits into a double discharge filament.

The rotation frequency and the number of discharge filaments of the kW-AC-ArMPT are further investigated. Under relatively low power (<600 W) conditions [Fig.5(A)], all the plasmas with different air contents are formed by a single filament, and the rotation frequency and microwave power are positively correlated. At the same power level, the increase in air content also facilitates the increase in the rotation frequency

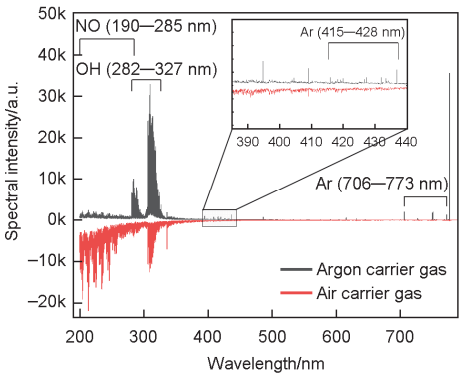

Fig.4 Spectra of argon carrier gas and air carrier gas plasma in the case of radial view under the same conditions

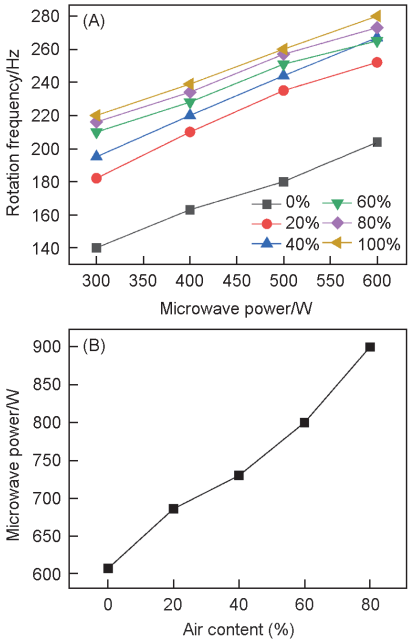

Fig.5 Trend of plasma rotation frequency with microwave power at different air contents (A) and threshold power for splitting into a double filament with different contents of the air in the mixed carrier gas (B)

of the plasma discharge filament. As Fig.5(B) shows, the threshold power for splitting into the double filament increases with the air content. In the process of turning the single filament structure into the double filament structure, the distance between the roots of the two filaments gradually expands. The double filament tends to be stable and symmetrical after a further increase in power. The possible reason for the transformation of the single filament into the double filament is that the power capacity of the single filament is limited. To carry more energy, the plasma filament splits, and the two filaments formed after the splitting together carry a larger microwave power. Compared with the single filament, the double filament can increase the spatial area of interaction between the sample and the plasma, thereby increasing the collision probability between the sample and the plasma filament at the atomic scale. Therefore, the double filament structure can effectively improve analytical performance[15].

3.2 Optical Diagnosis

Plasma temperature and electron number density are important physical parameters used describe the characteristics of plasma, which can help understand the plasma, thus laying a solid foundation for further improving plasma and improving its analytical performance.

Since the multiple transition probability of ferric in the excitation energy range is accurately known, ferric has become

https://doi.org/10.1007/s40242-023-3110-5

the most used thermometric species for measuring the excitation temperature (T_{exc})[16]. The ferric solution emission spectrum is obtained from the 50 ppm ferric chloride solution. The emission intensities of seven Fe (I) lines ranging from 371 nm to 377 nm (371.993, 373.486, 373.713, 374.826, 374.948, 375.823, 376.379 nm) are selected and the T_{exc} of the plasma is calculated from the Boltzmann slope method[17]. If each atomic energy level obeys the Boltzmann distribution, the spectral line intensity (I_{qp}) of the transition from upper energy level q to lower energy level p satisfies the following equation [Eq. (1)]:

$$I_{qp} = \frac{hc}{4\pi\lambda} n \frac{g_p A_{qp}}{U(T)} \exp\left(-\frac{E_p}{kT_{exc}}\right) \quad (1)$$

where h is the Planck constant, c is the lightspeed, λ is the wavelength, g_p is the statistical weight of the level p, A_{qp} is the transition probability from upper level p to lower level q, n is the total number density of atoms or ions to be studied, $U(T)$ is the partition function, E_p is the energy at the level p and k is the Boltzmann constant. Since all spectral lines emitted by the same excited state have the same value of $nhc/4\pi U(T)$, plotting $\ln(I_{qp}\lambda/g_pA_{qp})$ against E_p will give a straight line with a slope of $-1/kT_{exc}$. The corresponding Boltzmann graph is shown in Fig.6(A).

The electron number density (n_e) is estimated by the relative intensity of the spectral lines emitted by neutral and ionized atoms. In the experiment, the measurement of the n_e is carried out using the spectral information of the calcium element. The spectral signals of Ca (I) 422.673 nm and Ca (II) 396.847 nm are obtained from a 50 ppm calcium standard solution. And then n_e is calculated according to Saha equation [Eq. (2)]:

$$n_e = 4.83 \times 10^{15} \times \frac{I^0 g^+ A^+ \lambda^0}{I^+ g^0 A^0 \lambda^+} T^{\frac{3}{2}} \exp\left(\frac{E^0 - E^+ - E_i^0 + \Delta E_i^0}{kT}\right) \quad (2)$$

where 0, and + denote the parameters related to the neutral atom and the +1 valence ions of the first ionization level, respectively, E_i^0 is the ionization energy of neutral atoms, ΔE_i^0 is used to correct for the effect of charged particles in the plasma on the dissociation of free atoms, which is generally taken as 0.05 eV, and T=T_{exc} in the local region of the plasma. The calculated results are at the same level as n_e reported in the literature[18].

The rotation temperature (T_{rot}) characterizes the behavior of diatomic molecules in the plasma, which is generally considered to be approximately equal to the gas temperature. In this study, hydroxide (OH) emission lines in the range of 306—312 nm are used for the measurement of T_{rot}, where the OH comes from the water vapor in the air carrier gas. The relationship between OH spectral line and rotation temperature can be expressed by the following equation [Eq. (3)]:

$$\ln\left(\frac{I\lambda}{A}\right) = \ln(g'hc) - \frac{E}{kT_{rot}} \quad (3)$$

where g' is a constant in a certain emission band.

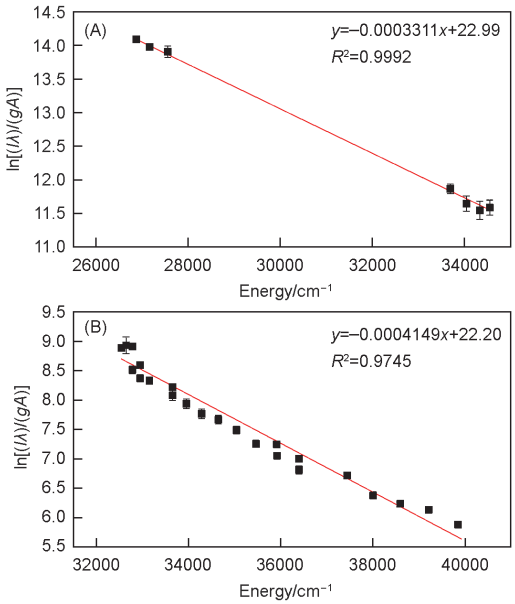

Fig.6 Boltzmann plot of ln($I\lambda/gA$) *vs*. energy made for T_{exc} measurement [the slope of this line is k_{slpoe}=−1/(0.69503×T_{exc})=−0.0003311] (A) and Boltzmann plot of ln($I\lambda/gA$) *vs*. energy made for T_{rot} measurement [the slope of this line is k_{slpoe}=−1/(0.69503×T_{rot})=−0.0004149] (B)

The corresponding graph is shown in Fig.6(B). All the T_{exc} and T_{rot} values mentioned above are the average values of three measurement results, with relative standard deviations less than 3% and 2.5%, respectively, while the coefficients of determination of all Boltzmann curves are greater than 0.98 and 0.95, separately. Under current conditions, the T_{exc} is calculated to be 4345^{+33}_{-45} K and the T_{rot} is 3468^{+40}_{-58} K.

The effects of air content on the plasma parameters (T_{rot}, T_{exc} and n_e) of kW-AC-ArMPT are shown in Fig.7. After adding air, the T_{rot} of the plasma had a significant rise, which becomes closer to the T_{exc} of the plasma, indicating that the addition of air contributes to the transition of the ArMPT into a local thermal equilibrium (LTE) state. The possible reasons are as follows. The introduction of air brings more diatomic molecules, and then a large number of activated nitrogen molecules N_2^* are produced through high-energy electron collision, nitrogen atom recombination, and argon metastable energy transfer. These activated nitrogen molecules can store excess energy in the form of rotational energy[19]. The effect of the introduction of air on the n_e is similar to the effect on the plasma temperature. The introduction of a small amount of air leads to a significant increase in the electron number density of the plasma. These phenomena have been observed in similar studies, such as the introduction of N_2 into the ICP source in Sesi's work[20], where a significant increase in n_e was observed, and in Zhang's work[21], where it was found that n_e of the microwave plasma increased with the proportion of N_2 in the N_2-Ar mixture.

https://doi.org/10.1007/s40242-023-3110-5

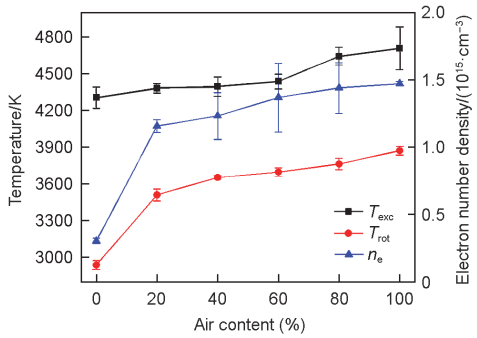

Fig.7 Effects of air content in the carrier gas on plasma parameters

The microwave power is 500 W and the carrier gas flow rate is 0.5 L/min.

The effects of microwave power on the plasma parameters are shown in Fig.8. A possible explanation for the increase in T_{rot} is that the increase in microwave power brings more energy, which aggravates the thermal motion of various molecules, atoms and charged particles in the plasma, and increases the chance of collision between free electrons and molecules. When the microwave power increases from 300 W to 700 W, the T_{exc} rises first and then decreases. Some scholars[22,23] have shown that there is a direct relationship between the T_{exc} and the power density of plasma. As the microwave power is increased beyond 500 W, the plasma volume expands rapidly, causing the power density to decrease, thus resulting in the decrease of T_{exc}. According to Fig.8, it can be found that n_e decreases continuously with the increase of microwave power, but the decrease is not large. Although increasing microwave power can bring more energy, which is beneficial to the increase in the number of electrons, it also leads to the rapid expansion of the plasma volume, and it is inferred that the volume expansion has a greater effect on the n_e in high power MPT, leading to a slow decrease in the n_e with the increase in microwave power. The better tolerance of air carrier gas at high power is due to the more sufficient energy of MPT with increased power, which can atomize and ionize air more effectively.

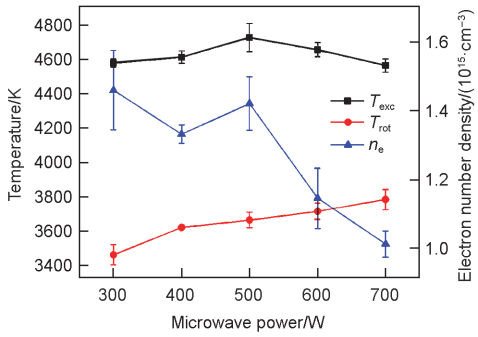

Fig.8 Effects of microwave power on plasma parameters

The carrier gas flow rate is 0.5 L/min and the air content is 100%.

The effects of carrier gas flow rate on the plasma parameters are shown in Fig.9. T_{rot} tends to fall due to the cooling effect caused by the increase of the carrier gas flow rate. The n_e continues to increase slightly, for reasons similar to the introduction of air.

The effect of the discharge filament structure on the plasma parameters is shown in Table 2. To minimize the influence of other factors on the experimental results, only the microwave power is adjusted in a small range to achieve changes in the structure of the plasma discharge filament (microwave power was set to 680 and 710 W, respectively).

Since the microwave power only changes by 30 W, it can be considered that the change of plasma parameters in this experiment is only related to the change of the discharge filament structure. The results in Table 2 show that when the plasma discharge filament is converted from a single discharge filament structure to a double discharge filament structure, the T_{exc} and T_{rot} of the plasma increase by about 100 K and the n_e of the plasma increases by nearly 10%. Yu[24] and Zhu[25] examined the elemental spectral emission intensity of Ca, Na, Cu and Cd in the state of a single discharge filament structure and a double discharge filament structure. It shows that the elemental spectral emission intensity obtained with the double discharge filament structure increases by 99.1%, 110.7%, 28.5%, and 10%, respectively. The increase in the number of filaments directly enhances the chance of collision between the sample aerosol and the filaments, and the efficiency of energy transfer, which greatly facilitates the evaporation, atomization and excitation processes of the sample aerosol and can effectively improve the detection performance.

Under different working conditions mentioned above, the T_{rot} is ranging from 3460 K to 3930 K, the T_{exc} is ranging from 3880 K to 5000 K and the n_e is ranging from 3.04×10^{14} cm^{-3}

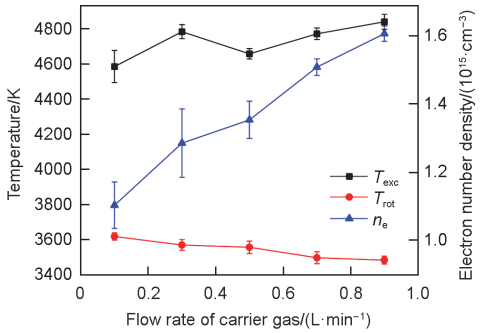

Fig.9 Effects of carrier gas flow rate on plasma parameters

The microwave power is 500 W and the air content is 100%.

Table 2 Effect of plasma discharge filament structure on T_{exc}, T_{rot} and n_e

Discharge structure	T_{exc}/K	T_{rot}/K	n_e/(10^{15}·cm^{-3})
Single filament	4636	3576	1.15
Double filament	4741	3660	1.28

https://doi.org/10.1007/s40242-023-3110-5

to 1.61×10^{15} cm^{-3}.

3.3 Detection Performance

When the power is 700 W and the air carrier gas flow rate is 0.6 L/min, we investigated the detection capability of the kW-AC-ArMPT for common heavy metal elements in polluted air, characterized by the detection limit of the corresponding elements. The standard curve is obtained according to the solutions of different concentration gradients of various elements, and then the solution detection limit of the elements is calculated.

The spectrometer (an echelle spectrometer ESA 4000, provided by LLA Instruments GmbH & Co. KG) can quickly obtain the spectral signal in the wavelength range of 200—780 nm with a resolution of 0.005 nm, which can meet the experimental requirements. The standard solutions of each heavy metal element (produced by Steel Research & Nanak Testing Technology Co., Ltd.) are diluted in a gradient manner by using secondary distilled deionized water according to the gradient dilution method. Eleven measurements are taken for each concentration of the sample and the mean value is calculated to plot the calibration curve. Secondary distilled deionized water is used as the blank sample to calculate the standard deviation.

Table 3 shows the detection limits of some heavy metal elements. Compared to the low power MPT with an air carrier gas flow rate of 0.2 L/min (200 W, other conditions are similar), kW-AC-MPT has similar detection limits for elements in Table 3. By increasing the microwave power, the introduction of higher flow rates of air carrier gas does not degrade the MPT's detection limit performance.

Table 3 Comparison of the detection limits of heavy metal elements in polluted air by different methods

Element	Detection limit/(ng·mL^{-1})	
	kW-AC-MPT	MPT[12]*
Cu	4.34	8.06
Ag	17.43	43.05
Cr	49.89	28.39
Zn	72.98	201.52
Ba	454.74	33.89
Hg	733.78	393.88
Pb	380.65	—

* Aerosol concentrations are used in this literature to calculate the detection limits. For comparison, the aerosol concentrations are converted to equivalent solution concentrations and the detection limits are recalculated.

4 Conclusions

In this study, the images and discharge filament behavior of the kW-AC-ArMPT are studied by the digital SLR and high-speed camera. Besides, the effects of different working conditions on the plasma electronic excitation temperature (T_{exc}), rotational temperature (T_{rot}), and electron number density (n_e) are studied by optical diagnostic methods. In addition, the detection limits of some elements are calculated. According to the results of the study, the following important conclusions have been drawn.

(1) The kW-ArMPT is extremely resistant to air introduction and can withstand at least 1.0 L/min of pure air injection. And the higher air carrier gas flow rate produces a more stable aerosol of micron-sized particles. It broadens the application prospect.

(2) Since T_{exc} is always much higher than T_{rot}, it is indicated that the kW-AC-ArMPT is still seriously deviating from the LTE state. However, adding air carrier gas and increasing the power can bring T_{exc} closer to T_{rot}, indicating that the improvement contributes to the transition of the kW-AC-ArMPT to the LTE state. Meanwhile, the overall volume of the plasma and the diameter of the central channel become larger, which is more conducive to the introduction of sample aerosol, and the T_{rot} and n_e of the plasma are increased, which has positive significance for sample evaporation and atomization.

(3) Besides, the detection limits of some heavy metal elements provided by kW-AC-ArMPT are in the ppb range.

The kW-AC-MPT can omit the process of sample pre-treatment and instead introduce ambient air and factory flue gas directly into the plasma for analysis by pumping. Therefore, it has potential for online and *in-situ* detection of ambient air quality and industrial exhaust gases.

Acknowledgements

This work was supported by the National Natural Science Foundation of China (No.62073287) and the Fund of Science and Technology Program of Huzhou, China (No.2021KT50).

Conflicts of Interest

The authors declare no conflicts of interest.

References

[1] Jin Q., Wang F., Hieftje G. M., *Chem. J. Chinese Universities*, **1990**, *11*, 1353
[2] Jin W., Yu B., Zhu D., Ying Y., Yu H., Jin Q., *Chem. J. Chinese Universities*, **2015**, *36* (11), 2157
[3] Yu B., Jin W., Zhu D., Ying Y., Yu H., Shan J., Xu C., Liu W., Jin Q., *Chem. Research in Chinese Universities*, **2016**, *32* (4), 549
[4] Zhu Z., Jiang T., Xiong X., Zou W., *Rapid Commun. Mass Spectrom.*, **2016**, *30*, 44
[5] Jiang T., Xiong X., Wang S., Luo Y., Fei Q., Yu A., Zhu Z., *Int. J. Mass Spectrom.*, **2016**, *399*, 33
[6] Jiang T., Jiang F., Zhuo Z., Liu H., Hu B., Li M., Li L., Huang Z., Zhou Z., Zhu Z., *Analyst*, **2021**, *146* (5), 1760
[7] Zeng L., Wu M., Chen S., Zheng R., Rao Y., He X., Duan Y., Wang X., *Talanta*, **2022**, *246*, 123516
[8] Jiang T., Peng Z., Xie M., Fang X., Hong Y., Huang Z., Gao W., Zhou Z., Li L., Zhu Z., *Anal. Methods*, **2020**, *12* (4), 535
[9] Yu D., Wei H., Li Y., Shao Y., Jin W., Yu B., *J. Anal. At. Spectrom.*, **2023**, *38* (7), 1402
[10] Ying Y., Jin W., Yu B., Liu S., Wu X., Yu H., Shan J., Zhu D., Jin Q., Mu Y., *Anal. Methods*, **2016**, *8*, 5079

[11] Ying Y., Jin W., Yan Y., Mu Y., Jin Q., *Chemometr. Intell. Lab. Syst.*, **2018**, *176*, 82
[12] Duan Y., Su Y., Jin Z., Abeln S. P., *Anal. Chem.*, **2000**, *72*, 1672
[13] Zhu D., Jin W., Yu B., Ying Y., Yu H., Shan J., Yan Y., Jin Q., *J. Anal. At. Spectrom.*, **2017**, *32*, 1595
[14] Yu B., Jin W., Ying Y., Yu H., Zhu D., Shan J., Liu W., Xu C., Jin Q., *J. Anal. At. Spectrom.*, **2016**, *31*, 759
[15] Jankowski K. J., Reszke E., *Microwave Induced Plasma Analytical Spectrometry*, Royal Society of Chemistry, London, **2010**
[16] Bruno B., Vincent G., Vincent M. R., Rosalba G., Marcella D. A., Alessandro D. G., *Spectrochim Acta Part B At. Spectrosc.*, **2023**, *204*, 106686
[17] Wang S., Li G., Zhou J., Jin Q., *Chem. Res. Chinese Universities*, **2006**, *22* (5), 560
[18] Jin Q., Zhang H., Yu A., Duan Y., Lu X., Wang F., *Anal. Sci.*, **1991**, *7*, 559
[19] Giersz J., Bartosiak M., Jankowski K. J., *J. Anal. At. Spectrom.*, **2017**, *32*, 1885
[20] Sesi N. N., MacKenzie A., Shanks K. E., Yang P., Hieftje G. M., *Spectrochim Acta Part B At. Spectrosc.*, **1994**, *49*, 1259
[21] Li S., Chen C., Zhang X., Zhang J., Wang Y., *Plasma Sources Sci. Technol.*, **2015**, *24*, 2
[22] Masamba W., Ali A. H., Winefordner J. D., *Spectrochim Acta Part B At. Spectrosc.*, **1992**, *47*, 481
[23] Goode S. R., Buddin N. P., Chambers B., Baughman K. W., Deavor J. P., *Spectrochim Acta Part B At. Spectrosc.*, **1985**, *40*, 317
[24] Yu B. W., *Research on Fundamental Theory of Microwave Plasma Torch (MPT) and Development of Kilowatt MPT Spectrometer*, Zhejiang University, Hangzhou, **2016**
[25] Zhu D., *Development of a Kilowatt Microwave Plasma Torch (MPT) Excitation Source for Atomic Emission Spectrometry*, Zhejiang University, Hangzhou, **2017**

https://doi.org/10.1007/s40242-023-3110-5